

Cite as: D. K. Simanshu *et al.*, *Science*  
10.1126/science.adq2004 (2025).

# BBO-10203 inhibits tumor growth without inducing hyperglycemia by blocking RAS-PI3K $\alpha$ interaction

Dhirendra K. Simanshu<sup>1\*†</sup>, Rui Xu<sup>2†</sup>, James P. Stice<sup>2</sup>, Daniel J. Czyzyk<sup>1</sup>, Siyu Feng<sup>2</sup>, John-Paul Denson<sup>1</sup>, Erin Riegler<sup>2</sup>, Yue Yang<sup>3</sup>, Cathy Zhang<sup>2</sup>, Sofia Donovan<sup>2</sup>, Brian P. Smith<sup>1</sup>, Maria Abreu-Blanco<sup>1</sup>, Ming Chen<sup>2</sup>, Cindy Feng<sup>2</sup>, Lijuan Fu<sup>2</sup>, Dana Rabara<sup>1</sup>, Lucy C Young<sup>4</sup>, Marcin Dyba<sup>1</sup>, Wupeng Yan<sup>1</sup>, Ken Lin<sup>2</sup>, Samar Ghorbanpoorvalukolaie<sup>5</sup>, Erik K. Larsen<sup>1</sup>, Wafa Malik<sup>5</sup>, Allison Champagne<sup>1</sup>, Katie Parker<sup>5</sup>, Jin Hyun Ju<sup>6</sup>, Stevan Jeknic<sup>6</sup>, Dominic Esposito<sup>1</sup>, David M. Turner<sup>1</sup>, Felice C. Lightstone<sup>3</sup>, Bin Wang<sup>2</sup>, Paul M. Wehn<sup>2</sup>, Keshi Wang<sup>2</sup>, Andrew G. Stephen<sup>1</sup>, Anna E. Maciag<sup>1</sup>, Aaron N. Hata<sup>5</sup>, Kerstin W. Sinkevicius<sup>2</sup>, Dwight V. Nissley<sup>1</sup>, Eli M. Wallace<sup>2</sup>, Frank McCormick<sup>1,4\*</sup>, Pedro J. Beltran<sup>2\*</sup>

<sup>1</sup>NCI RAS Initiative, Cancer Research Technology Program, Frederick National Laboratory for Cancer Research, Leidos Biomedical Research, Inc., Frederick, MD, USA.

<sup>2</sup>BridgeBio Oncology Therapeutics, South San Francisco, CA, USA. <sup>3</sup>Physical and Life Sciences Directorate, Lawrence Livermore National Laboratory, Livermore, CA, USA.

<sup>4</sup>Helen Diller Family Comprehensive Cancer Center, University of California San Francisco, San Francisco, CA, USA. <sup>5</sup>Massachusetts General Hospital Cancer Center, Boston, MA, USA, and Department of Medicine, Massachusetts General Hospital and Harvard Medical School, Boston, MA, USA. <sup>6</sup>BridgeBio Pharma, San Francisco, CA, USA.

\*Corresponding author. E-mail: dhirendra.simanshu@nih.gov (D.K.S.); frank.mccormick@ucsf.edu (F.M.); pedro.beltran@bridgebiooncology.com (P.J.B.).

†These authors contributed equally to this work.

**BBO-10203 is an orally available drug that covalently and specifically binds to the RAS-binding domain of phosphoinositide 3-kinase  $\alpha$  (PI3K $\alpha$ ), preventing its activation by HRAS, NRAS, and KRAS. It inhibited PI3K $\alpha$  activation in tumors with oncogenic mutations in KRAS or PIK3CA, and in tumors with human epidermal growth factor receptor 2 (HER2) amplification or overexpression. In preclinical models, BBO-10203 caused significant tumor growth inhibition across multiple tumor types and showed enhanced efficacy in combination with inhibitors of cyclin-dependent kinase 4/6 (CDK4/6), estrogen receptor (ER), HER2 and KRAS-G12C mutant, including in tumors harboring mutations in Kelch-like ECH-associated protein 1 (KEAP1) and Serine/Threonine Kinase 11 (STK11). Notably, these antitumor effects occurred without inducing hyperglycemia, as insulin signaling does not depend on RAS-mediated PI3K $\alpha$  activation to promote glucose uptake.**

Phosphoinositide 3-kinases function in many aspects of cell physiology, including growth, differentiation, survival, and migration. PI3K $\alpha$  is regulated by receptor tyrosine kinases and contributes to insulin homeostasis. The catalytic subunit of PI3K $\alpha$ , p110 $\alpha$  (encoded by the *PIK3CA* gene), is recruited to activated receptors through its direct interaction with the PI3K $\alpha$  regulatory subunit p85, or in the case of insulin and insulin-like growth factor 1 (IGF-1), through p85 binding to insulin receptor substrate (IRS) proteins (1). Deletion of p110 $\alpha$  causes embryonic lethality (2), whereas mice heterozygous for p110 $\alpha$  survive but are glucose intolerant and suffer from hyperinsulinemia and hyperphagia, among other phenotypes associated with defective insulin signaling (1).

Lipid kinase activity associated with v-Src and polyomavirus middle T oncoproteins (3–6) led to the identification of PI 3-kinase (7). Subsequently, three classes and multiple isoforms of PI 3-kinases were characterized. An oncogenic form of PI 3-kinase  $\alpha$  (*PIK3CA*) was discovered in an avian retrovirus (8), and activating mutations in *PIK3CA* were later identified in human tumors (9). These mutations occur in 24–46% of endometrial cancers, 20–32% of breast cancers, 20–27% of bladder cancers, and at notable frequencies in most other cancer types (10).

Canonical RAS proteins bind directly to PI 3-kinases (11) but with lower affinity than to RAF kinases (12). Oncogenic RAS proteins activate PI3K $\alpha$  when overexpressed (13). Furthermore, disrupting RAS-PI3K $\alpha$  interaction through mutations T208D and K227A in the PI3K $\alpha$  RAS-binding domain (RBD) severely impairs tumor formation driven by KRAS-G12D (14). Systemic disruption of RAS-PI3K $\alpha$  interaction in mice is well tolerated and does not provoke hyperglycemia (15). Tumors driven by oncogenic mutants of EGFR regress after genetic disruption of RAS-PI3K $\alpha$  binding (15), and neo-angiogenesis is impaired (16). These findings indicate that RAS binding to PI3K $\alpha$  is not essential in normal cells, or for insulin homeostasis, but is vital for tumor formation and maintenance.

We describe an orally available drug, BBO-10203, that phenocopies the PI3K $\alpha$  T208D-K227A mutant. It binds covalently to PI3K $\alpha$  near the RAS binding site, and blocks its interaction with the canonical RAS proteins HRAS, NRAS, and KRAS. It is effective in multiple mouse models and, importantly, does not affect insulin homeostasis.

### BBO-10203 binds covalently and specifically to p110 $\alpha$

The crystal structures of MRAS, RRAS2, and KRAS bound to p110 $\alpha$  have been solved, with the KRAS-p110 $\alpha$  complex stabilized by a molecular glue compound D927 (17). Figure 1A shows a structure of KRAS bound to non-hydrolyzable GTP analog (GMPPNP) in complex with p110 $\alpha$ , highlighting its interaction primarily through the RBD (PDB: 9C15). RAS binding to the p110 $\alpha$  RBD does not alter the conformation of the kinase domain, supporting a proposed model where RAS activates PI3K $\alpha$  by stabilizing contacts between the p110 $\alpha$  and the plasma membrane, where the substrate phosphatidylinositol 4,5-bisphosphate (PIP2) resides, without affecting kinase activity directly or allosterically (17–19).

Compound D927, used to crystallize the KRAS-p110 $\alpha$  complex, was identified through phenotypic screening for anti-diabetic compounds (20). It functions as a molecular glue by enhancing RAS-p110 $\alpha$  interactions (17). Structural analysis revealed that D927 binds by inducing a pocket in the p110 $\alpha$  RBD, with its aniline moiety interacting with KRAS residues Y40 and R41 (17). Given this structural insight, we tested whether substituting the flexible aniline group in D927 with a rigid moiety linked to the pyridazine ring would sterically clash with KRAS Y40, thereby disrupting the KRAS-p110 $\alpha$  interaction (fig. S1). Structure-based drug design and molecular modeling led to the discovery of compound **1**, which breaks instead of stabilizes the KRAS-p110 $\alpha$  interaction. A considerable increase in cell potency was achieved by introducing an acrylamide electrophile that specifically targets the native cysteine C242 in the p110 $\alpha$  RBD binding pocket, leading to compound **2**. Subsequent optimization of potency and pharmacokinetic properties led to the development candidate BBO-10203.

BBO-10203 (Fig. 1B) covalently binds to p110 $\alpha$ , as determined by MALDI-TOF mass spectrometry (Fig. 1C and fig. S2). The crystal structure of PI3K $\alpha$  RBD complexed with BBO-10203 shows covalent engagement with C242 via an acrylamide warhead (Fig. 1D and table S1). Key residues in PI3K $\alpha$  RBD that interact with BBO-10203 include Q205, Y207, I225, K228, Y246, and Y250 (fig. S3), which are adjacent to mutations T208D and K227A known to disrupt RAS-p110 $\alpha$  binding (14). Figure 1E shows that BBO-10203, covalently bound to PI3K $\alpha$ , would sterically clash with KRAS, preventing its binding.

BBO-10203 is specific for PI3K $\alpha$  and exhibits no affinity for the other three PI3K isoforms: PI3K $\beta$ , PI3K $\delta$ , and PI3K $\gamma$  (fig. S4A). Comparisons of the sequence and structure of the RBD of PI3K $\alpha$  with the other three PI3K isoforms elucidate this specificity. The other isoforms have deletions in this region and differ at critical residues within the binding site, and the cysteine (C242) to which BBO-10203 binds covalently is present only in the  $\alpha$  isoform (Fig. 1, F and G).

KRAS binds to p110 $\alpha$  with a  $K_D$  of 17  $\mu$ M under

physiological salt and pH conditions (Fig. 1H), decreasing to 2.2  $\mu$ M under lower salt and pH conditions (17, 21), as measured using isothermal titration calorimetry. BBO-10203, covalently bound to the p110 $\alpha$  RBD, completely blocked KRAS binding (Fig. 1H), with similar effects observed for HRAS and NRAS (fig. S4, B and C). BBO-10203 blocked the interaction of KRAS-G12D with PI3K $\alpha$  in human embryonic kidney (HEK) 293T cells with an  $IC_{50}$  of 6 nM but did not affect KRAS-G12D binding to the protein kinase CRAF (Fig. 1I). Covalent modification of p110 $\alpha$  by BBO-10203 did not alter its kinase activity in vitro (Fig. 1J), unlike the PI3K $\alpha$  inhibitor alpelisib, which binds in the ATP pocket and potently inhibits kinase activity (18).

### Responses to BBO-10203 in specific cell genotypes

BBO-10203 inhibited the PI3K $\alpha$  pathway, as indicated by reduced phosphorylation of protein kinase AKT in multiple cell lines (Fig. 2A and table S2). Responses clustered into three groups: a non-response group characterized by PTEN loss, an intermediate group that includes KRAS-G12X mutations and mutations in *PIK3CA* (helical or kinase domains), and a highly responsive group with HER2 amplification. Figure 2B shows that most HER2-amplified cell lines showed near-complete inhibition of phosphorylated AKT (pAKT) by BBO-10203 with  $IC_{50}$  values below 10 nM (table S2).

The inhibited growth of HER2-amplified tumors by BBO-10203 was unexpected. Inhibition of the interaction between RAS proteins and PI3K $\alpha$  causes regressions in tumors driven by activated EGFR, suggesting that RAS activation of PI3K $\alpha$  might extend beyond KRAS mutant cancers (15). However, multiple noncanonical RAS-related proteins, including RRAS, RRAS2, and MRAS, can activate PI3K $\alpha$  (13, 22), and it is not known which proteins are important in this context. The effects of BBO-10203 on pAKT and cell viability were less pronounced in cells driven by receptor tyrosine kinases other than HER2. In HER2-amplified tumors, canonical RAS proteins have been excluded (23), suggesting other non-canonical RAS proteins are involved in this process. The extent to which multiple non-canonical RAS proteins may be involved in each cell line, along with the ability of BBO-10203 to inhibit them, might be responsible for the heterogeneity observed within the group. Regardless of the precise mechanism, the effects of BBO-10203 on these cells are quite strong and suggest a potential role in treating patients suffering from tumors of this genotype.

Hotspot mutations in *PIK3CA* occur in the helical and kinase domains. Kinase domain mutations, particularly H1047R, are considered less dependent on RAS than helical domain mutations (E542K or E545K) (8). In our panel of cell lines, both classes of mutation responded to BBO-10203, although kinase domain mutants were indeed less sensitive (Fig. 2C and table S2).

We tested a panel of human cell lines with KRAS mutations and observed pAKT inhibition ranging from 40% to 70% (Fig. 2D and table S2). The incomplete response could result from partial target engagement or due to RAS-independent pathways leading to PI3K $\alpha$  activation. To test these possibilities, we developed a target engagement assay measuring free p110 $\alpha$  after exposure to BBO-10203, revealing complete or near-complete engagement across all genotypes genotype (Fig. 2E). Specifically, target engagement was observed in the PTEN-null glioblastoma cell line U87-MG, where pAKT remained unaffected; in the GP2d pancreatic cancer (KRAS-G12D), NCI-H358 lung cancer (KRAS-G12C), and MCF7 breast cancer (PI3K $\alpha$ -E545K) cell lines, where pAKT was partially reduced; and in the BT-474 breast cancer cell line with HER2 amplification, where pAKT was completely inhibited. We conclude that variations in response to BBO-10203 reflect varying dependencies on RAS proteins for PI3K $\alpha$  activation.

We compared BBO-10203 to RMC-6236, which inhibits active canonical RAS proteins HRAS, NRAS, and KRAS (24). In four KRAS G12 mutant cell lines, both compounds produced highly similar responses, particularly in terms of  $E_{\max}$ , representing the maximum inhibition achievable, regardless of dose. In contrast, RMC-6236 had little effect on cell lines with HER2 amplification, where BBO-10203 completely inhibited pAKT, suggesting that PI3K $\alpha$  activation in these cells likely depends on non-canonical RAS proteins (Fig. 2F). In a breast cancer cell line, MCF7, which has a PI3K $\alpha$  helical domain mutation (E545K), both RMC-6236 and BBO-10203 caused partial reduced pAKT levels, indicating RAS-independent signaling. In another breast cancer cell line, T47D, harboring a PI3K $\alpha$  kinase domain mutation (H1047R), BBO-10203 similarly produced a partial response, whereas RMC-6236 had no effect, further implicating contributions from non-canonical RAS proteins to PI3K $\alpha$  signaling (Fig. 2G).

In all the cell lines tested, alpelisib inhibited AKT activity completely only at concentrations 1  $\mu$ M or higher. At these concentrations, alpelisib not only targets PI3K $\alpha$  but also effectively inhibits PI3-kinase  $\delta$  and  $\gamma$  isoforms (21). These data indicate that inhibition of multiple PI3K isoforms is necessary for complete inhibition of AKT activity (22). In most cases, BBO-10203 inhibited PI3K $\alpha$  signaling more potently than alpelisib but did not achieve complete inhibition of AKT activity ( $E_{\max}$ ) because its effect only reflects inhibition of RAS-driven PI3K $\alpha$  activity. Despite differences in mechanism, potency, and  $E_{\max}$ , when alpelisib was used at concentrations mostly selective for PI3K $\alpha$ , RNA Seq analysis and Western blot analysis revealed almost identical changes in global transcription and post-translational downstream signaling. The similarities confirm that BBO-10203, like alpelisib at concentrations below 1  $\mu$ M, does indeed act through inhibition of PI3K $\alpha$  (figs. S5 and S6). Furthermore, BBO-10203 showed excellent selectivity in the Eurofins Discovery

SafetyScreen44, KINOMEscan screening panel, and cellular cysteine profiling assays (figs. S7 and S8). The specificity of BBO-10203 for C242 on PI3K $\alpha$  was further assessed using a NanoBioluminescence Resonance Energy Transfer (NanoBRET) protein-protein interaction assay. BBO-10203 showed strong activity in disrupting the interaction between PI3K $\alpha$  and KRAS, with an IC<sub>50</sub> of 3 nM (fig. S9). When the C242 in PI3K $\alpha$  was mutated to a serine, BBO-10203 no longer potently inhibited the PI3K $\alpha$  (C242S): KRAS interaction, with an IC<sub>50</sub> of 2000 nM, a 650-fold decrease in potency.

### Target engagement in vivo and effects on glucose uptake

BBO-10203 demonstrated good oral bioavailability in mice with a dose-proportional increase in plasma levels, enabling its evaluation in xenograft tumor models (fig. S10). BBO-10203 inhibited accumulation of pAKT in the KYSE-410 CDX model of esophageal squamous cell carcinoma, in a dose-dependent manner from 3 to 100 mg/kg and showed sustained inhibition over 24 hours at 30 and 100 mg/kg (Fig. 3A). A single 30 mg/kg dose of BBO-10203 achieved complete target engagement in KYSE-410 tumors as measured in a Western blot-based streptavidin mass shift (SMaSh) assay (Fig. 3B). Dose-dependent and effective anti-tumor activity was observed after daily oral treatment with BBO-10203 in the KYSE-410 CDX model, with tumor regression observed at 30 mg/kg (Fig. 3C). Both the KRAS-G12C inhibitor sotorasib and the HER2 kinase inhibitor tucatinib showed minimum efficacy in this model, and the PI3K $\alpha$  kinase inhibitor alpelisib led to tumor stasis at the clinically relevant dose of 20 mg/kg (fig. S11).

The PI3K $\alpha$  kinase inhibitor alpelisib is FDA-approved for treating hormone receptor-positive (HR+), HER2-negative (HER-) breast cancer in which the *PIK3CA* is mutated (25). Despite its efficacy in tumors expressing mutated *PIK3CA*, alpelisib also inhibits wild-type PI3K $\alpha$ , resulting in significant on-target side effects, including hyperglycemia. BBO-10203 does not provoke hyperglycemia, because insulin signaling to PI3K $\alpha$  does not depend on RAS (26). Figure 3D shows that in an oral glucose tolerance test, glucose accumulates in a dose-dependent manner in mice treated with alpelisib, but mice treated with 100 mg/kg of BBO-10203 (3 times the efficacious dose) show no accumulation of glucose and no increase in serum c-peptide (Fig. 3E). C-peptide measurements are a commonly used surrogate for insulin measurements due to the short half-life of insulin (27).

### BBO-10203 causes tumor regression in combination with targeted therapies

BBO-10203 caused tumor regressions in the KYSE-410 model, but in most models, combinations of treatments are required to achieve tumor regression. Increased pAKT signaling provides acute resistance to multiple targeted therapies such as

trastuzumab in HER2-positive (HER2+) breast cancer patients, ER antagonists and CDK4/6 inhibitors in HR+ HER2-breast cancer patients, and KRAS-G12C inhibitors in non-small cell lung cancer (NSCLC) patients with KRAS-G12C mutant tumors.

Combinations of BBO-10203 with these standard-of-care therapies are predicted to prevent pAKT-driven resistance while being well-tolerated. A combination of BBO-10203 with the HER2 inhibitor trastuzumab caused inhibition of cell proliferation at concentrations of each agent that are ineffective on their own (Fig. 4A). Near complete and sustained inhibition of pAKT for 72 hours was achieved by the combination of these agents, without affecting p110 $\alpha$  expression (Fig. 4B). Similar results were achieved in another HER2-amplified cell line, ZR-75-30, with the same combination. BBO-10203 was also effective in combination with the ER antagonist fulvestrant, the CDK4/6 inhibitor palbociclib, and a novel KRAS-G12C ON inhibitor, BBO-8520 (Fig. 4, C and D) (28).

Analysis of PI3K $\alpha$  inhibitors in cell lines may underrepresent their potential as therapeutics in vivo, because growth in vitro often provokes activation of PI3K $\alpha$  through integrin engagement. Therefore, we tested the combinations described above in xenograft models. Tumor stasis or regressions were achieved in the selected representative models in combination with trastuzumab, fulvestrant, palbociclib, or BBO-8520 (Fig. 5, A to C).

To evaluate the mechanism of action driving the efficacy in the NCI-H2122 CDX model, BBO-10203 and BBO-8520 were dosed alone or in combination. Although amounts of bromodeoxyuridine (a measure of cell proliferation) significantly decreased and amounts of cleaved caspase-3 increased 6 hours after a single dose of BBO-10203, the combination of BBO-10203 and BBO-8520 exhibited much larger effects at both 6 hours and 24 hours. These results demonstrated that BBO-10203 has tumor intrinsic effects on cell proliferation and survival, and the combination with a KRAS-G12C inhibitor enhances these effects (Fig. 5D).

## Summary

Mutations in *PIK3CA* occur frequently in cancer along with driver oncogenes and, in model systems, potentiate driver activity. For example, the expression of an activated allele of *PIK3CA* accelerates the onset and penetrance of tumors driven by BRAF-V600E in mice (29). In another example, treatment of mice with KRAS-G12D-driven tumors using PI3K inhibitors demonstrated synergy with MEK inhibitors in reducing established tumors (30). We show that BBO-10203 combined with KRAS inhibitors causes the regression of tumors unresponsive to KRAS inhibitors alone, including those with KEAP1/STK11 mutations. We also observed tumor regression in response to BBO-10203 in combination with drugs targeting CDK4/6, ER, and HER2. BBO-10203 achieved

these effects without detectable toxicity and, most importantly, without provoking hyperglycemia. In tumors with HER2 amplification, BBO-10203 completely inhibited PI3K $\alpha$ , revealing a pathway essential for tumor cell survival, likely involving a non-canonical RAS protein. BBO-10203 is currently being tested in patients and is expected to provide substantial clinical benefits through a differentiated mechanism that alleviates toxicities that have previously restricted use of PI3K $\alpha$  inhibitors.

## REFERENCES AND NOTES

1. L. C. Foukas, M. Claret, W. Pearce, K. Okkenhaug, S. Meek, E. Peskett, S. Sancho, A. J. H. Smith, D. J. Withers, B. Vanhaesebroeck, Critical role for the p110 $\alpha$  phosphoinositide-3-OH kinase in growth and metabolic regulation. *Nature* **441**, 366–370 (2006). doi:10.1038/nature04694 Medline
2. L. Bi, I. Okabe, D. J. Bernard, A. Wynshaw-Boris, R. L. Nussbaum, Proliferative defect and embryonic lethality in mice homozygous for a deletion in the p110 $\alpha$  subunit of phosphoinositide 3-kinase. *J. Biol. Chem.* **274**, 10963–10968 (1999). doi:10.1074/jbc.274.16.10963 Medline
3. Y. Sugimoto, M. Whitman, L. C. Cantley, R. L. Erikson, Evidence that the Rous sarcoma virus transforming gene product phosphorylates phosphatidylinositol and diacylglycerol. *Proc. Natl. Acad. Sci. U.S.A.* **81**, 2117–2121 (1984). doi:10.1073/pnas.81.7.2117 Medline
4. I. G. Macara, G. V. Marinetti, P. C. Balduzzi, Transforming protein of avian sarcoma virus UR2 is associated with phosphatidylinositol kinase activity: Possible role in tumorigenesis. *Proc. Natl. Acad. Sci. U.S.A.* **81**, 2728–2732 (1984). doi:10.1073/pnas.81.9.2728 Medline
5. D. R. Kaplan, M. Whitman, B. Schaffhausen, L. Raptis, R. L. Garcea, D. Pallas, T. M. Roberts, L. Cantley, Phosphatidylinositol metabolism and polyoma-mediated transformation. *Proc. Natl. Acad. Sci. U.S.A.* **83**, 3624–3628 (1986). doi:10.1073/pnas.83.11.3624 Medline
6. M. Whitman, D. R. Kaplan, B. Schaffhausen, L. Cantley, T. M. Roberts, Association of phosphatidylinositol kinase activity with polyoma middle-T competent for transformation. *Nature* **315**, 239–242 (1985). doi:10.1038/315239a0 Medline
7. M. Whitman, C. P. Downes, M. Keeler, T. Keller, L. Cantley, Type I phosphatidylinositol kinase makes a novel inositol phospholipid, phosphatidylinositol-3-phosphate. *Nature* **332**, 644–646 (1988). doi:10.1038/332644a0 Medline
8. H. W. Chang, M. Aoki, D. Fruman, K. R. Auger, A. Bellacosa, P. N. Tsichlis, L. C. Cantley, T. M. Roberts, P. K. Vogt, Transformation of chicken cells by the gene encoding the catalytic subunit of PI 3-kinase. *Science* **276**, 1848–1850 (1997). doi:10.1126/science.276.5320.1848 Medline
9. Y. Samuels, Z. Wang, A. Bardelli, N. Silliman, J. Ptak, S. Szabo, H. Yan, A. Gazdar, S. M. Powell, G. J. Riggins, J. K. V. Willson, S. Markowitz, K. W. Kinzler, B. Vogelstein, V. E. Velculescu, High frequency of mutations of the *PIK3CA* gene in human cancers. *Science* **304**, 554 (2004). doi:10.1126/science.1096502 Medline
10. R. Arafeh, Y. Samuels, *PIK3CA* in cancer: The past 30 years. *Semin. Cancer Biol.* **59**, 36–49 (2019). doi:10.1016/j.semcancer.2019.02.002 Medline
11. P. Rodriguez-Viciana, P. H. Warne, R. Dhand, B. Vanhaesebroeck, I. Gout, M. J. Fry, M. D. Waterfield, J. Downward, Phosphatidylinositol-3-OH kinase as a direct target of Ras. *Nature* **370**, 527–532 (1994). doi:10.1038/370527a0 Medline
12. H. Nakhaeizadeh, E. Amin, S. Nakhaei-Rad, R. Dvorsky, M. R. Ahmadian, The RAS-Effector Interface: Isoform-Specific Differences in the Effector Binding Regions. *PLOS ONE* **11**, e0167145 (2016). doi:10.1371/journal.pone.0167145 Medline
13. P. Rodriguez-Viciana, C. Sabatier, F. McCormick, Signaling specificity by Ras family GTPases is determined by the full spectrum of effectors they regulate. *Mol. Cell. Biol.* **24**, 4943–4954 (2004). doi:10.1128/MCB.24.11.4943-4954.2004 Medline
14. S. Gupta, A. R. Ramjaun, P. Haiko, Y. Wang, P. H. Warne, B. Nicke, E. Nye, G. Stamp, K. Alitalo, J. Downward, Binding of ras to phosphoinositide 3-kinase p110 $\alpha$  is required for ras-driven tumorigenesis in mice. *Cell* **129**, 957–968 (2007). doi:10.1016/j.cell.2007.03.051 Medline

15. M. M. Murillo, S. Rana, B. Spencer-Dene, E. Nye, G. Stamp, J. Downward, Disruption of the Interaction of RAS with PI 3-Kinase Induces Regression of EGFR-Mutant-Driven Lung Cancer. *Cell Rep.* **25**, 3545–3553.e2 (2018). [doi:10.1016/j.celrep.2018.12.003](https://doi.org/10.1016/j.celrep.2018.12.003) [Medline](#)
16. M. M. Murillo, S. Zelenay, E. Nye, E. Castellano, F. Lassailly, G. Stamp, J. Downward, RAS interaction with PI3K p110 $\alpha$  is required for tumor-induced angiogenesis. *J. Clin. Invest.* **124**, 3601–3611 (2014). [doi:10.1172/JCI74134](https://doi.org/10.1172/JCI74134) [Medline](#)
17. D. Czyzyk, W. Yan, S. Messing, W. Gillette, T. Tsuji, M. Yamaguchi, S. Furuzono, D. M. Turner, D. Esposito, D. V. Nissley, F. McCormick, D. K. Simanshu, Structural insights into isoform-specific RAS-PI3K $\alpha$  interactions and the role of RAS in PI3K $\alpha$  activation. *Nat. Commun.* **16**, 525 (2025). [doi:10.1038/s41467-024-55766-x](https://doi.org/10.1038/s41467-024-55766-x) [Medline](#)
18. M. Zhang, H. Jang, R. Nussinov, PI3K inhibitors: Review and new strategies. *Chem. Sci.* **11**, 5855–5865 (2020). [doi:10.1039/D0SC01676D](https://doi.org/10.1039/D0SC01676D) [Medline](#)
19. T. C. Buckles, B. P. Ziemba, G. R. Masson, R. L. Williams, J. J. Falke, Single-Molecule Study Reveals How Receptor and Ras Synergistically Activate PI3K $\alpha$  and PIP<sub>3</sub> Signaling. *Biophys. J.* **113**, 2396–2405 (2017). [doi:10.1016/j.bpj.2017.09.018](https://doi.org/10.1016/j.bpj.2017.09.018) [Medline](#)
20. T. Tsuji, M. Yamaguchi, J. Kuroyanagi, S. Furuzono, M. Konishi, K. Terayama, J. Tanaka, M. Saito, Y. Kobayashi, Discovery of novel pyridazine derivatives as glucose transporter type 4 (GLUT4) translocation activators. *Bioorg. Med. Chem. Lett.* **29**, 1785–1790 (2019). [doi:10.1016/j.bmcl.2019.05.013](https://doi.org/10.1016/j.bmcl.2019.05.013) [Medline](#)
21. N. G. Martinez, D. F. Thieker, L. M. Carey, J. A. Rasquinha, S. K. Kistler, B. A. Kuhlman, S. L. Campbell, Biophysical and Structural Characterization of Novel RAS-Binding Domains (RBDs) of PI3K $\alpha$  and PI3K $\gamma$ . *J. Mol. Biol.* **433**, 166838 (2021). [doi:10.1016/j.jmb.2021.166838](https://doi.org/10.1016/j.jmb.2021.166838) [Medline](#)
22. C. Fritsch, A. Huang, C. Chatenay-Rivauday, C. Schnell, A. Reddy, M. Liu, A. Kauffmann, D. Guthy, D. Erdmann, A. De Pover, P. Furet, H. Gao, S. Ferretti, Y. Wang, J. Trappe, S. M. Brachmann, S.-M. Maira, C. Wilson, M. Boehm, C. Garcia-Echeverria, P. Chene, M. Wiesmann, R. Cozens, J. Lehar, R. Schlegel, G. Caravatti, F. Hofmann, W. R. Sellers, Characterization of the novel and specific PI3K $\alpha$  inhibitor NVP-BYL719 and development of the patient stratification strategy for clinical trials. *Mol. Cancer Ther.* **13**, 1117–1129 (2014). [doi:10.1158/1535-7163.MCT-13-0865](https://doi.org/10.1158/1535-7163.MCT-13-0865) [Medline](#)
23. A. Ruiz-Saenz, C. Dreyer, M. R. Campbell, V. Steri, N. Gulizia, M. M. Moasser, HER2 Amplification in Tumors Activates PI3K/Akt Signaling Independent of HER3. *Cancer Res.* **78**, 3645–3658 (2018). [doi:10.1158/0008-5472.CAN-18-0430](https://doi.org/10.1158/0008-5472.CAN-18-0430) [Medline](#)
24. J. Jiang, L. Jiang, B. J. Maldonato, Y. Wang, M. Holderfield, I. Aronchik, I. P. Winters, Z. Salman, C. Blaj, M. Menard, J. Brodbeck, Z. Chen, X. Wei, M. J. Rosen, Y. Gindin, B. J. Lee, J. W. Evans, S. Chang, Z. Wang, K. J. Seamon, D. Parsons, J. Cregg, A. Marquez, A. C. A. Tomlinson, J. K. Yano, J. E. Knox, E. Quintana, A. J. Aguirre, K. C. Arbour, A. Reed, W. C. Gustafson, A. L. Gill, E. S. Koltun, D. Wildes, J. A. M. Smith, Z. Wang, M. Singh, Translational and Therapeutic Evaluation of RAS-GTP Inhibition by RMC-6236 in RAS-Driven Cancers. *Cancer Discov.* **14**, 994–1017 (2024). [doi:10.1158/2159-8290.CD-24-0027](https://doi.org/10.1158/2159-8290.CD-24-0027) [Medline](#)
25. T. Wilhoit, J. M. Patrick, M. B. May, Alpelisib: A Novel Therapy for Patients With PIK3CA-Mutated Metastatic Breast Cancer. *J. Adv. Pract. Oncol.* **11**, 768–775 (2020). [Medline](#)
26. C. Taha, A. Klip, The insulin signaling pathway. *J. Membr. Biol.* **169**, 1–12 (1999). [doi:10.1007/PL00005896](https://doi.org/10.1007/PL00005896) [Medline](#)
27. E. Leighton, C. A. Sainsbury, G. C. Jones, A Practical Review of C-Peptide Testing in Diabetes. *Diabetes Ther.* **8**, 475–487 (2017). [doi:10.1007/s13300-017-0265-4](https://doi.org/10.1007/s13300-017-0265-4) [Medline](#)
28. A. E. Maciag, J. Stice, B. Wang, A. Sharma, A. Chan, K. Lin, D. Singh, M. Dyba, Y. Yang, S. Setoodeh, B. P. Smith, D. Rabara, Z. Zhang, E. K. Larsen, D. Esposito, J. P. Denson, M. Ranieri, M. Meynardie, S. Mehdizadeh, P. Alexander, M. A. Blanco, D. Turner, R. Xu, F. C. Lightstone, K. K. Wong, D. Simanshu, K. Wang, A. G. Stephen, K. Sinkevicius, D. V. Nissley, E. Wallace, F. McCormick, P. J. Beltran, Abstract ND07: BBO-8520, a first-in-class, direct inhibitor of KRASG12C (ON), locks GTP-bound KRASG12C in the state 1 conformation resulting in rapid and complete blockade of effector binding. *Cancer Res.* **84** (suppl. 7), ND07 (2024). [doi:10.1158/1538-7445.AM2024-ND07](https://doi.org/10.1158/1538-7445.AM2024-ND07)
29. R. P. Charles, J. Silva, G. Iezza, W. A. Phillips, M. McMahon, Activating BRAF and PIK3CA mutations cooperate to promote anaplastic thyroid carcinogenesis. *Mol. Cancer Res.* **12**, 979–986 (2014). [doi:10.1158/1541-7786.MCR-14-0158-T](https://doi.org/10.1158/1541-7786.MCR-14-0158-T) [Medline](#)
30. J. A. Engelman, L. Chen, X. Tan, K. Crosby, A. R. Guimaraes, R. Upadhyay, M. Maira, K. McNamara, S. A. Perera, Y. Song, L. R. Chirieac, R. Kaur, A. Lightbown, J. Simendinger, T. Li, R. F. Padera, C. Garcia-Echeverria, R. Weissleder, U. Mahmood, L. C. Cantley, K.-K. Wong, Effective use of PI3K and MEK inhibitors to treat mutant Kras G12D and PIK3CA H1047R murine lung cancers. *Nat. Med.* **14**, 1351–1356 (2008). [doi:10.1038/nm.1890](https://doi.org/10.1038/nm.1890) [Medline](#)
31. R. Xu, B. Wang, E. Wallace, P. Wehn, P. J. Beltran, J. Stice, K. Sinkevicius, Y. Yang, P. Bisignano, F. Lightstone, D. K. Simanshu, D. M. Turner, D. J. Czyzyk, S. Singh, J. R. Yerabolu, F. McCormick, WIPO patent WO2023154282A1 (2023).
32. B. Wang, R. Xu, E. Wallace, Z. Zhang, D. M. Turner, A. E. Maciag, D. K. Simanshu, A. H. Chan, T. Liao, C. J. Brassard, Y. Yang, P. Bisignano, F. Lightstone, WIPO patent WO2023004102A2 (2022).
33. M. J. Whitley, T. H. Tran, M. Rigby, M. Yi, S. Dharmiah, T. J. Waybright, N. Ramakrishnan, S. Perkins, T. Taylor, S. Messing, D. Esposito, D. V. Nissley, F. McCormick, A. G. Stephen, T. Turbyville, G. Cornilescu, D. K. Simanshu, Comparative analysis of KRAS4a and KRAS4b splice variants reveals distinctive structural and functional properties. *Sci. Adv.* **10**, ead4137 (2024). [doi:10.1126/sciadv.adj4137](https://doi.org/10.1126/sciadv.adj4137) [Medline](#)
34. F. Weissmann, G. Petzold, R. VanderLinden, P. J. Huis In 't Veld, N. G. Brown, F. Lampert, S. Westermann, H. Stark, B. A. Schulman, J.-M. Peters, biGbac enables rapid gene assembly for the expression of large multisubunit protein complexes. *Proc. Natl. Acad. Sci. U.S.A.* **113**, E2564–E2569 (2016). [doi:10.1073/pnas.1604935113](https://doi.org/10.1073/pnas.1604935113) [Medline](#)
35. T. Taylor, J. P. Denson, D. Esposito, Optimizing Expression and Solubility of Proteins in E. coli Using Modified Media and Induction Parameters. *Methods Mol. Biol.* **1586**, 65–82 (2017). [doi:10.1007/978-1-4939-6887-9\\_5](https://doi.org/10.1007/978-1-4939-6887-9_5) [Medline](#)
36. A. C. Nelson, T. J. Turbyville, S. Dharmiah, M. Rigby, R. Yang, T.-Y. Wang, J. Columbus, R. Stephens, T. Taylor, D. Sciacca, G. Onsongo, A. Sarver, S. Subramanian, D. V. Nissley, D. K. Simanshu, E. Lou, RAS internal tandem duplication disrupts GTPase-activating protein (GAP) binding to activate oncogenic signaling. *J. Biol. Chem.* **295**, 9335–9348 (2020). [doi:10.1074/jbc.RA119.011080](https://doi.org/10.1074/jbc.RA119.011080) [Medline](#)
37. K. Kopra, E. Vuorinen, M. Abreu-Blanco, Q. Wang, V. Eskonen, W. Gillette, A. T. Pulliainen, M. Holderfield, H. Härmä, Homogeneous Dual-Parametric-Coupled Assay for Simultaneous Nucleotide Exchange and KRAS/RAF-RBD Interaction Monitoring. *Anal. Chem.* **92**, 4971–4979 (2020). [doi:10.1021/acs.analchem.9b05126](https://doi.org/10.1021/acs.analchem.9b05126) [Medline](#)
38. W. Kabsch, Xds. *Acta Crystallogr. D* **66**, 125–132 (2010). [doi:10.1107/S0907444909047337](https://doi.org/10.1107/S0907444909047337) [Medline](#)
39. D. Liebschner, P. V. Afonine, M. L. Baker, G. Bunkóczi, V. B. Chen, T. I. Croll, B. Hintze, L.-W. Hung, S. Jain, A. J. McCoy, N. W. Moriarty, R. D. Oeffner, B. K. Poon, M. G. Prisant, R. J. Read, J. S. Richardson, D. C. Richardson, M. D. Sammito, O. V. Sobolev, D. H. Stockwell, T. C. Terwilliger, A. G. Urzhumtsev, L. L. Videau, C. J. Williams, P. D. Adams, Macromolecular structure determination using X-rays, neutrons and electrons: Recent developments in Phenix. *Acta Crystallogr. D* **75**, 861–877 (2019). [doi:10.1107/S2059798319011471](https://doi.org/10.1107/S2059798319011471) [Medline](#)
40. P. D. Adams, P. V. Afonine, G. Bunkóczi, V. B. Chen, I. W. Davis, N. Echols, J. J. Headd, L.-W. Hung, G. J. Kapral, R. W. Grosse-Kunstleve, A. J. McCoy, N. W. Moriarty, R. Oeffner, R. J. Read, D. C. Richardson, J. S. Richardson, T. C. Terwilliger, P. H. Zwart, PHENIX: A comprehensive Python-based system for macromolecular structure solution. *Acta Crystallogr. D* **66**, 213–221 (2010). [doi:10.1107/S0907444909052925](https://doi.org/10.1107/S0907444909052925) [Medline](#)
41. P. Emsley, B. Lohkamp, W. G. Scott, K. Cowtan, Features and development of Coot. *Acta Crystallogr. D* **66**, 486–501 (2010). [doi:10.1107/S0907444910007493](https://doi.org/10.1107/S0907444910007493) [Medline](#)
42. T. C. Terwilliger, R. W. Grosse-Kunstleve, P. V. Afonine, N. W. Moriarty, P. D. Adams, R. J. Read, P. H. Zwart, L.-W. Hung, Iterative-build OMIT maps: Map improvement by iterative model building and refinement without model bias. *Acta Crystallogr. D* **64**, 515–524 (2008). [doi:10.1107/S0907444908004319](https://doi.org/10.1107/S0907444908004319) [Medline](#)
43. E. Jurrus, D. Engel, K. Star, K. Monson, J. Brandi, L. E. Felberg, D. H. Brookes, L. Wilson, J. Chen, K. Liles, M. Chun, P. Li, D. W. Gohara, T. Dolinsky, R. Konecny, D. R. Koes, J. E. Nielsen, T. Head-Gordon, W. Geng, R. Krasny, G.-W. Wei, M. J. Holst, J. A. McCammon, N. A. Baker, Improvements to the APBS biomolecular solvation software suite. *Protein Sci.* **27**, 112–128 (2018). [doi:10.1002/pro.3280](https://doi.org/10.1002/pro.3280) [Medline](#)

44. A. Morin, B. Eisenbraun, J. Key, P. C. Sanschagrin, M. A. Timony, M. Ottaviano, P. Sliz. Collaboration gets the most out of software. *eLife* **2**, e01456 (2013). [doi:10.7554/eLife.01456](https://doi.org/10.7554/eLife.01456) [Medline](#)
45. A. Subramanian, P. Tamayo, V. K. Mootha, S. Mukherjee, B. L. Ebert, M. A. Gillette, A. Paulovich, S. L. Pomeroy, T. R. Golub, E. S. Lander, J. P. Mesirov. Gene set enrichment analysis: A knowledge-based approach for interpreting genome-wide expression profiles. *Proc. Natl. Acad. Sci. U.S.A.* **102**, 15545–15550 (2005). [doi:10.1073/pnas.0506580102](https://doi.org/10.1073/pnas.0506580102) [Medline](#)
46. Z. Fang, X. Liu, G. Peltz, GSEAPy: A comprehensive package for performing gene set enrichment analysis in Python. *Bioinformatics* **39**, btac757 (2023). [doi:10.1093/bioinformatics/btac757](https://doi.org/10.1093/bioinformatics/btac757) [Medline](#)

## ACKNOWLEDGMENTS

We thank Bill Gillette, Simon Messing, Matthew Drew, Carissa Grose, and their colleagues from the RAS Initiative at the Frederick National Laboratory for their assistance in preparing recombinant proteins. We thank the support from the Lawrence Livermore National Laboratory's institutional grand challenge program. **Funding:** The X-ray crystallography work is based on research conducted at the NE-CAT beamlines, funded by NIH/NIGMS (P30 GM124165). The Eiger 16M detector on 24-ID-E is funded by an NIH-ORIP HEI grant (S100D021527). This research utilizes resources from the Advanced Photon Source, a U.S. Department of Energy (DOE) Office of Science User Facility operated by Argonne National Laboratory under Contract No. DE-AC02-06CH11357. This project has been funded in part with federal funds from the National Cancer Institute, National Institutes of Health, under Contract No. 75N91019D00024, and Lawrence Livermore National Laboratory under Contract No. DE-AC52-07NA27344 (Release: LLNL-JRNL-863848). The content of this publication does not necessarily reflect the views or policies of the Department of Health and Human Services, nor does mention of trade names, commercial products, or organizations imply endorsement by the U.S. government. **Author contributions:** Conceptualization: DKS, FM, DVN, RX, PJB, EMW. Methodology: BW, CF, DJC, ER, KL, MA-B, MD, PMW, PJB, SF, SG, SD, YY. Investigation: DJC, SF, ER, CZ, AC, BPS, LF, CF, DR, EKL, J-PD, KP, LCY, MC, MD, SG, SD, SJ, WM, WY, YY. Resources: DVN, EMW, PJB, ANH, FCL, FM. Formal Analysis: RX, DKS, KS, JJ, JPS, SF, SG, CZ, DJC, ANH, PJB. Supervision: KS, DKS, RX, JPS, KL, AEM, AGS, DE, DMT, KW, SF, ANH, FCL, DVN, EMW, PJB, FM. Project administration: DKS, RX, DVN, PJB, EMW. Writing – original draft: FM, PJB, DKS, RX. Writing – review and editing: FM, PJB, DKS, RX, EMW, DVN. **Competing interests:** All BridgeBio Oncology Therapeutics (BBOT) authors are employees and stockholders of BBOT, a private company. FM is a consultant for Amgen, Daiichi Sankyo Ltd., Exuma Biotech, Ideaya Biosciences, and Quanta Therapeutics. FM is a consultant and co-founder (with ownership interest, including stock options) of BridgeBio. FM serves as the scientific advisor for the National Cancer Institute RAS Initiative at the Frederick National Laboratory for Cancer Research/Leidos Biomedical Research, Inc. FM has received research grants from Daiichi Sankyo and Gilead Sciences and serves as the Principal Investigator for research agreements with Boehringer Ingelheim and Roche. ANH has received research grants from BridgeBio, Amgen, Bristol-Myers Squibb, C4 Therapeutics, Eli Lilly, Novartis, Nuvalent, Pfizer, and Scorpion Therapeutics, and has served as a compensated consultant for Amgen, Engine Biosciences, Nuvalent, Oncovalent, Pfizer, Tigenix, and Tolremo Therapeutics. RX, BW, EMW, PMW, PJB, JPS, KS, YY, FCL, DKS, DMT, DJC, and FM are co-inventors on a patent application titled "Compounds having a T-structure formed by at least four cycles for use in the treatment of cancer and other indications," application number WO2023/154282. The other authors declare no competing interests. **Data and materials availability:** The atomic coordinates and structure factors of the PI3K $\alpha$ -RBD covalently bound to BBO-10203 have been deposited in the Protein Data Bank and can be accessed using the accession number 9B4U. **License information:** Copyright © 2025 the authors, some rights reserved; exclusive licensee American Association for the Advancement of Science. No claim to original US government works. <https://www.science.org/about/science-licenses-journal-article-reuse>

## SUPPLEMENTARY MATERIALS

[science.org/doi/10.1126/science.adq2004](https://www.science.org/doi/10.1126/science.adq2004)

Materials and Methods  
 Figures S1 to S11  
 Tables S1 and S2  
 References (31–46)  
 MDAR Reproducibility Checklist

Submitted 6 May 2024; resubmitted 25 November 2024

Accepted 14 March 2025

Published online 12 June 2025

10.1126/science.adq2004



**Fig. 1. BBO-10203 covalently binds PI3K $\alpha$ -RBD, preventing interaction with HRAS, KRAS, and NRAS.** (A) Structure of the KRAS-p110 $\alpha$  complex (PDB: 9C15), stabilized by glue D927 showing interaction between p110 $\alpha$ -RBD (cyan) and KRAS (wheat). The C2, helical, and kinase domains are colored yellow, blue, and green, respectively. (B) Chemical structure of BBO-10203. (C) Mass chromatogram of PI3K $\alpha$ -RBD covalently labeled with BBO-10203 after 30 min; a minor peak at 17569.5 m/z is a MALDI matrix artifact generated during ionization. (D) Crystal structure of PI3K $\alpha$ -RBD (cyan, cartoon) covalently labeled with BBO-10203 (pink, ball and stick). Key PI3K $\alpha$  residues interacting with BBO-10203 are illustrated in stick representation. (E) Model of KRAS in complex with PI3K $\alpha$ -RBD covalently bound to BBO-10203 shows steric clash between BBO-10203 and KRAS Y40. (F) Superposition of the RBD structures of PI3K $\alpha$ , PI3K $\beta$ , PI3K $\delta$ , and PI3K $\gamma$  highlights differences at the BBO-10203 binding site. (G) Sequence alignment of the RBDs of all four PI3K isoforms shows deletions and lack of conservation of key residues (indicated by triangles above the aligned sequences), which form the BBO-10203 binding pocket in PI3K $\alpha$ . (H) ITC measurements showing the binding affinity of KRAS (GMPPNP) for both unlabeled and BBO-10203-labeled forms of PI3K $\alpha$ . (I) BBO-10203 disrupts the interaction between KRAS-G12D and p110 $\alpha$ , with an IC<sub>50</sub> of 6 nM. HEK 293T cells were transfected with 3XFLAG-KRAS-G12D. Twenty-four hours later, cells were treated for 2 hours with BBO-10203. Following immunoprecipitation with anti-FLAG antibodies, Western blots were probed for endogenous p110 $\alpha$  and CRAF. A representative blot from n=3 replicates is shown. Below: Dose-response curve of p110 $\alpha$  bound to KRAS using quantification of Western blot bands. (J) PI3K $\alpha$  kinase activity assay comparing BBO-10203 and alpelisib. Dose titration of inhibitors was tested with recombinant PI3K $\alpha$ , lipid substrate, and ATP, measuring ATP/ADP conversion via luciferase activity, reported as percent activity.

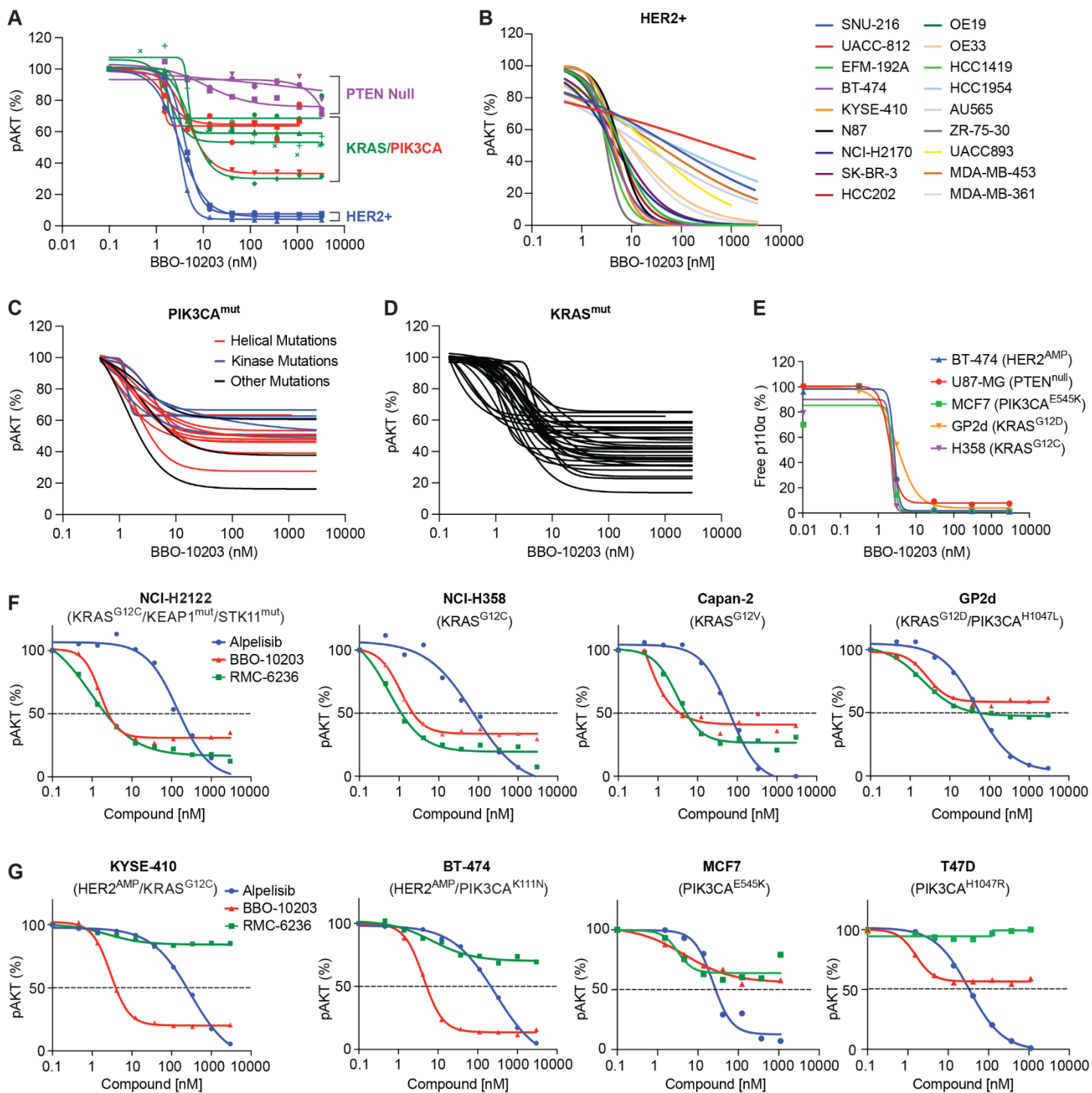


**Fig. 2. BBO-10203 activity in various cell lines with diverse cancer genotypes.** (A) Inhibition of phospho-AKT by BBO-10203 in cancer cell lines carrying different genetic variations, including PTEN loss-of-function mutations (magenta), HER2 amplification (blue), *PIK3CA* mutations (red), and *KRAS* mutations (green). (B) Inhibition of phospho-AKT by BBO-10203 in HER2-amplified or overexpressing cancer cell lines. (C) Inhibition of phospho-AKT by BBO-10203 in *PIK3CA*-mutated cancer cell lines, encompassing helical domain mutations (red), kinase domain mutations (blue), and others (black). (D) Inhibition of phospho-AKT by BBO-10203 in *KRAS*-mutated cancer cell lines. (E) Target engagement of P110 $\alpha$  by BBO-10203 in cancer cell lines with different genotypes, including HER2-amplified, *KRAS*-G12X, PTEN-null, and *PIK3CA*-mutated, using a customized Meso Scale Discovery (MSD) assay to measure the unbound fraction of p110 $\alpha$ . (F) Inhibition of phospho-AKT by BBO-10203 (red), the PI3K $\alpha$  kinase inhibitor alpelisib (blue), and the RAS(ON) inhibitor RMC-6236 (green) in *KRAS*-mutated cancer cell lines, including NCI-H2122 (G12C), NCI-H358 (G12C), Capan-2 (G12V), and GP2d (G12D). (G) Inhibition of phospho-AKT by BBO-10203 (red), the PI3K $\alpha$  kinase inhibitor alpelisib (blue), and the RAS(ON) inhibitor RMC-6236 (green) in HER2-amplified or *PIK3CA*-mutated cancer cell lines, including KYSE-410 (HER2<sup>AMP</sup>), BT-474 (HER2<sup>AMP</sup>), MCF7 (Helical<sup>E545K</sup>), and T47D (Kinase<sup>H1047R</sup>).

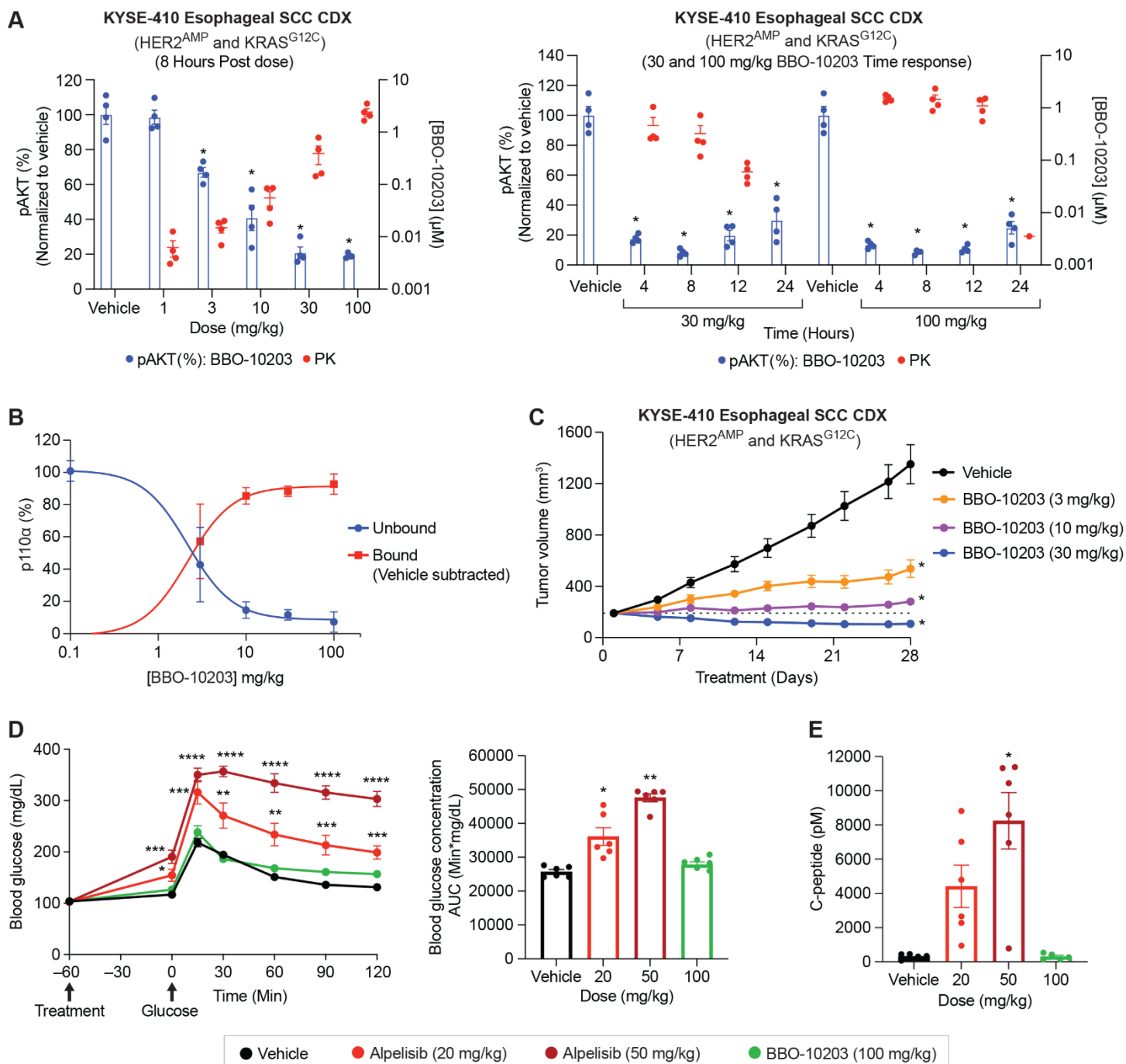


**Fig. 3. Inhibition of PI3K $\alpha$  activity without inducing hyperglycemia.** (A) Tumor pAKT levels in KYSE-410 tumor-bearing mice at the indicated time points after a single dose of the indicated levels of vehicle or BBO-10203. The indicated groups showed statistically significant inhibition of pAKT compared to the vehicle group (\* $p < 0.0001$ ). (B) p110 $\alpha$  target engagement of BBO-10203 in KYSE-410 tumors was measured via a Western blot-based band-shift SmaSh assay. A dose-dependent response in p110 $\alpha$  target engagement was observed 8 hours after dosing. (C) KYSE-410 tumor-bearing mice were dosed with the indicated levels of vehicle or BBO-10203. All treatment groups exhibited statistically significant anti-tumor activity compared to the vehicle group (\* $p < 0.0001$ ). (D) An oral glucose tolerance test (OGTT) was conducted with fasted male C57BL/6 mice following a single dose of the indicated levels of vehicle, alpelisib, or BBO-10203. The indicated groups demonstrated a statistically significant increase in blood glucose concentrations compared to the vehicle group at each timepoint (\* $p < 0.05$ , \*\* $p < 0.01$ , \*\*\* $p < 0.001$ , \*\*\*\* $p < 0.0001$ ) (left panel) and in blood glucose concentration AUC compared to the vehicle group (\* $p < 0.001$ , \*\* $p < 0.0001$ ) (right panel). (E) Serum c-peptide levels were measured from the mice in (D) at 150 min following the glucose dose. The indicated groups showed a statistically significant increase in c-peptide levels compared to the vehicle group (\* $p < 0.001$ ).

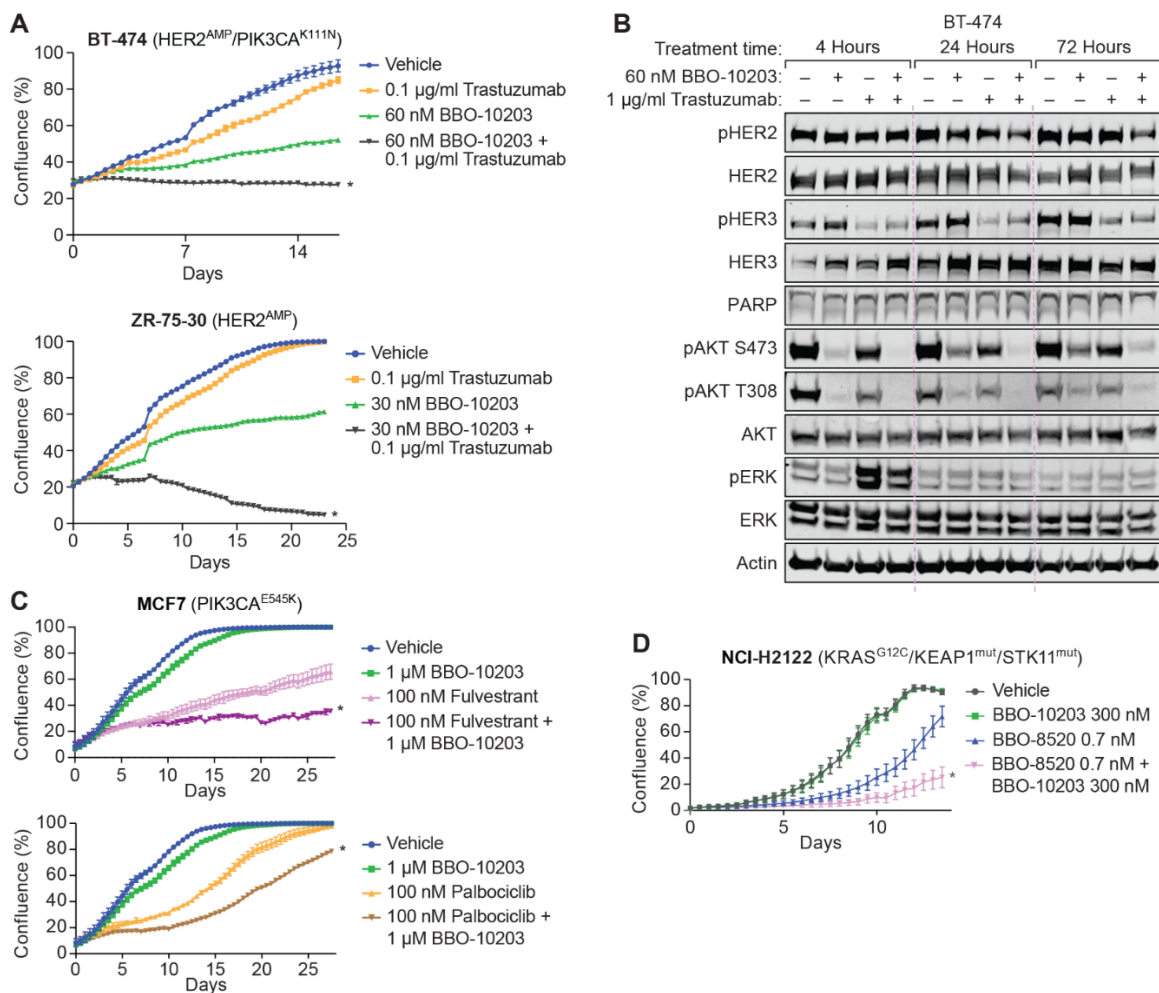


**Fig. 4. In vitro activity of BBO-10203 in combination with multiple agents.** (A) Growth inhibition from mono- and combination therapies of BBO-10203 and trastuzumab was assessed in clonogenic assays using HER2+ cancer cell lines BT474 and ZR-75-30. Cell confluence was measured every 12 hours on an Incucyte S3 imaging system for continuous 2-3 weeks. For panels 4A, 4C, and 4D, confluence ( $\pm$  SEM) with two-way repeated measures ANOVA followed by a Tukey multiple comparison test showed that the indicated treatment groups had a statistically significant activity for the combination treatment compared to each respective monotherapy ( $*p < 0.001$ ). (B) Western blot analysis of the upstream and downstream signaling changes of PI3K/AKT and MAPK pathways at various time points post-treatment with BBO-10203, trastuzumab, or a combination of both. (C) Growth inhibition from mono- and combination therapies of BBO-10203 with fulvestrant or palbociclib was evaluated in clonogenic assays using the ER+/HER2-/PIK3CA-E545K cancer cell line MCF7. Cell confluence was measured every 12 hours on an Incucyte S3 imaging system for four weeks continuously. (D) Growth inhibition from mono- and combination therapies of BBO-10203 with the KRAS-G12C (ON) inhibitor BBO-8520 was assessed in clonogenic assays using the cancer cell line NCI-H2122. Cell confluence was measured every 12 hours continuously for two weeks on an Incucyte S3 imaging system.

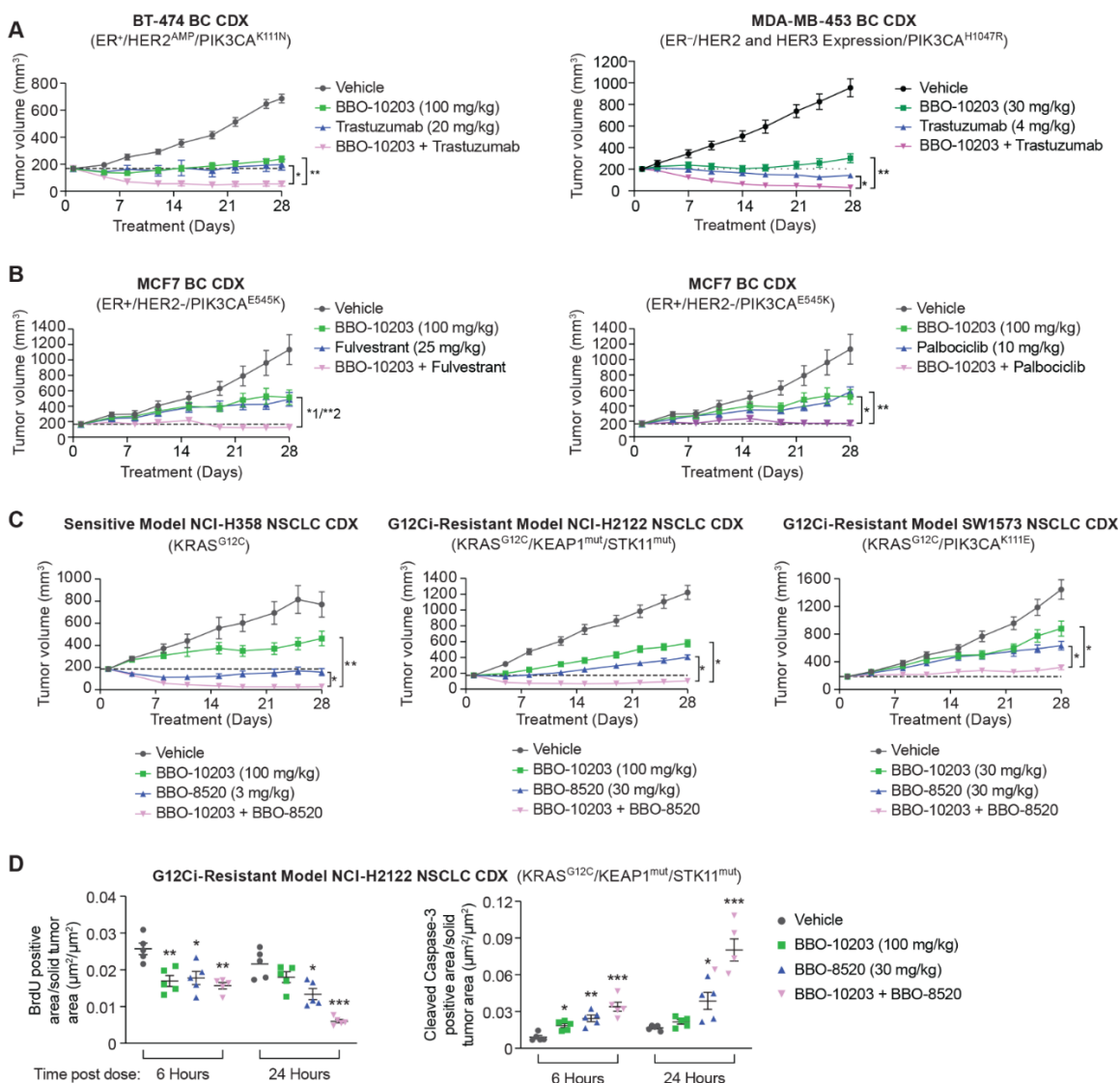


**Fig. 5. In vivo activity of BBO-10203 in combination with multiple agents.** (A) BT-474 (left panel) or MDA-MB-453 (right panel) tumor-bearing mice were dosed with the indicated levels of vehicle, BBO-10203, trastuzumab, or the combination of BBO-10203 and trastuzumab. The indicated monotherapy vs combination groups had a statistically significant difference in anti-tumor activity from day 5 to 28 (\* $p < 0.05$ ; \*\* $p < 0.0001$ ) (left panel) and from day 3 to 28 (\* $p < 0.01$ ; \*\* $p < 0.001$ ) (right panel). (B) MCF7 tumor-bearing mice were dosed with the indicated levels of vehicle, BBO-10203, fulvestrant, or the combination of BBO-10203 and fulvestrant (left panel), or with vehicle, BBO-10203, palbociclib, or the combination of BBO-10203 and palbociclib (right panel). The indicated monotherapy vs combination groups had a statistically significant difference in anti-tumor activity from day 5 to 28 [\* $p < 0.01$  (1: fulvestrant) and \*\* $p < 0.001$  (2: BBO-10203) (left panel); (\* $p < 0.01$ , \*\* $p < 0.001$ ) (right panel)]. (C) NCI-H358 (left panel), NCI-H2122 (middle panel), and SW1573 (right panel) tumor-bearing mice were dosed with the indicated levels of vehicle, BBO-10203, BBO-8520, or the combination of BBO-10203 and BBO-8520. The indicated monotherapy vs combination groups had a statistically significant difference in anti-tumor activity from day 4 to 28 (\* $p < 0.01$ , \*\* $p < 0.0001$ ) (right panel), from day 5 to 28 (\* $p < 0.0001$ ) (middle panel), and from day 4 to 28 (\* $p < 0.001$ ) (left panel). (D) Tumor levels of BrdU (left panel) and cleaved caspase-3 (right panel) were measured from NCI-H2122 tumor-bearing mice at 6 or 24 hours after a single dose of the indicated levels of vehicle, BBO-10203, BBO-8520, or the combination of BBO-10203 and BBO-8520. The indicated groups had a statistically significant change in levels compared to the vehicle group [(\*) $p < 0.01$ , \*\* $p < 0.001$ , \*\*\* $p < 0.0001$ ) (left panel); (\* $p < 0.05$ , \*\* $p < 0.001$ , \*\*\* $p < 0.0001$ ) (right panel)].